Artificial neural-network based model to forecast the electrical and thermal efficiencies of PVT air collector systems

Y. Chaibi, M. Malvoni, T. El Rhafiki, Tarik Kousksou, Y. Zeraouli

Artificial Neural-Network based model to forecast the electrical and thermal efficiencies of PVT air collector systems

Y. Chaibi [1,*], M. Malvoni [2], T. El Rhafiki [1], T. Kousksou [1], Y. Zeraouli [1]

[1] Université de Pau et des Pays de l'Adour, E2S UPPA, SIAME, Pau, France
[2] School of Electrical and Computer Engineering, National Technical University of Athens, 15780 Athens, Greece

Corresponding author:
E-mail address: chaibi.yassine@gmail.com
y.chaibi@edu.umi.ac.ma

Abstract

In the recent decade, Machine Learning techniques have been widely deployed in solar systems due their high accuracy in predicting the performances without going through the physical modelling. In this work, the Artificial Neural Network (ANN) method is adopted to forecast the electrical and thermal efficiencies of a photovoltaic/thermal (PVT) air collector system. Indeed, two accurate modelling techniques have been used to generate the output results for training and validation. Both deployed electrical and thermal models have been validated experimentally and demonstrated high accuracy. Then, real climatic samples of one year with a 10 minute step of the Jordan valley location have been adopted to generate the electrical and thermal efficiencies. These latter are used in the training and validation of the developed ANN model under various combinations of the weather variables. The solar irradiance and the module temperature are the most important variables to consider as input in a NN-based model respectively. The developed ANN model shows MAE of 0.0078% and 3.3607% in predicting the electrical and thermal efficiency respectively. The electrical efficiency can be predicted with higher accuracy than the thermal efficiency. Further, the results demonstrate that the ANN outperforms the LS-SVM in forecasting the PVT air collector performances.

Keywords: *Artificial neural network; PVT air collector; electrical model; thermal model; performance forecasting;*

1. Introduction

Controlling global energy consumption over recent decades is becoming a central issue in discussions on climate change and the global task to reduce carbon emissions (Yilmaz et al., 2019). Today, renewable energy systems and energy efficiency are acclaimed by the International Energy Agency (IEA) as a key driver of economic growth, reducing emissions and boosting the energy security of countries (IEA PVPS, 2019). More specifically, solar-based energy systems demonstrated a good compromise between the investment cost and efficiency. According to the IEA, the electricity generation using solar energy systems achieved a remarkable growth in the last decade (IEA PVPS, 2019).

One of the most effective solutions to reduce the consumption of electrical energy is the development and implementation of hybrid solar systems that can generate two useful products simultaneously. The PVT system is an interesting technology as it combines photovoltaic and thermal systems, generating electrical and thermal energy simultaneously (Rejeb et al., 2020). Most popular PVT systems are designed with a cooling fluid flowing in an open-loop (usually air) (Yang and Athienitis, 2014) or a closed-loop (usually water) (Yu et al., 2019), but there are also other PVT collectors using an hybrid cooling system of air and water (Su et al., 2016). Water-based PVT systems are more efficient than air-based PVT systems due to its high thermo-physical properties (Abdelrazik et al., 2018).

Over the last years, a significant number of research projects on PVT technology have been carried-out and various synthesis papers on PVT systems have been published (Kumar et al., 2015). Several authors have been interested in PVT air collectors due to their low-manufacturing costs (Diwania et al., 2020). Air cooling system provides a simple and economical solution for cooling the photovoltaic modules. Air can be heated to various temperature levels and its circulation can be either forced (via a fan) or natural (Chaibi et al., 2021). Forced circulation is required due to a better heat transfer by convection and conduction, however, the fan power consumption decreases the net electricity gain (Ibrahim et al., 2011).

The development of physical models is necessary to analyze and study the electrical and thermal performances of PVT air systems (Kumar et al., 2015). In the literature, the electrical behavior of PVT air systems has been imitated using equivalent-circuit models. Waliullah et al. used the double-diode model to compute the output power of a PVT air system (Waliullah

et al., 2015). The results are compared to the experiments and shown a remarkable disagreement, which is explained by the climatic data inaccuracy. Tarabsheh et al. adopted the single-diode configuration to evaluate the PVT air system performances under different ranges of temperature. The obtained results demonstrate the accuracy of this model by taking into account the temperature gradient overall the PV module surface, and it was reported that cooling PV cells enhances the electrical performances (Al Tarabsheh et al., 2016). Other configurations of electrical models have been adopted in PVT air systems (Babu and Ponnambalam, 2018) in order to forecast the electrical performances especially the electrical efficiency.

A number of thermal models have been developed to study the thermal performance of PVT air systems (Touafek et al., 2013). Most of the models are generic or based on electrical analogy using thermal resistance to describe the heat transfers between the different layers constituting the system (Agrawal and Tiwari, 2013). Tonui et al. developed a physical model of an air PVT system using the analogy with the solar thermal collector model and experimental results. The model allows the calculation of the thermal and electrical efficiencies of the solar collector without requiring precise knowledge of its composition and without involving thermodynamic modelling (Tonui and Tripanagnostopoulos, 2008, 2007). In addition, the most of the physical models developed in the literature assume that the temperature is uniform at each layer of the system and does not vary according to the airflow direction (Barone et al., 2019). Such models are unable to predict the effects of the thermal gradient along each layer on the thermal performance of the system.

In the last decades, predicting the performances of PVT systems by using artificial intelligence becomes a key solution to avoid simulating the mathematical models and to overcome their limitations. Accordingly, the advantages of reducing the computing time and to get high prediction accuracy are the main reasons to adopt the use of machine learning algorithms. In the literature, many studies have been conducted to forecast the electrical (Maria and Yassine, 2020); and thermal efficiencies of PVT systems (Mojumder et al., 2017). Caner et al. used 80 samples recorded of two solar air collectors to build an ANN-based model in order to predict the thermal efficiency. The results were satisfactory comparing to the experiments (Caner et al., 2011). In the same context, Varol et al. adopted the ANN, the Adapted-Network-Based Fuzzy Interference System (ANFIS) and the Support Vector Machine (SVM) methods to forecast the thermal performances of a phase change material in solar collectors. The results demonstrated the high performance of the SVM technique (Varol

et al., 2010). Also, Ahmadi et al. proposed two models based on ANN and Least Squares SVM methods to predict the electrical and thermal efficiencies of a PVT system. The results shown that the LS-SVM represented the best performances (Ahmadi et al., 2019).

Most of reported studies about forecasting the electrical and thermal efficiencies adopted a limited number of samples in the training and the validation processes, due to the unavailability of experimental samples. The main contribution of this paper is the implementing of an ANN based model to determine the electrical and thermal efficiencies of air collector PVT systems. In this work the novelty is represented by the development of a new and original accurate electrical model together with an original detailed transient thermal model of PVT air system, by which it is possible to determine the temperature evolution in each layer as a function of the system length. Further, the adopted data for the training and the validation processes refer to 1 year of real climatic conditions of Jordan valley location with a step of 30 minute. This overcome the limitation of previous studies, which used a limited number of samples to train and test the neural network. Different combinations of the weather variables were considered to assess the performance of the NN-based model to predict the electrical and thermal efficiencies, demonstrating that the choice of the variables as input of the neural network is very important to perform a model with low error. The developed ANN model is also compared with the LS-SVM method in order to confirm the high accuracy in predicting the electrical and thermal efficiencies of the PVT air systems.

This manuscript is arranged as follows: First, the followed methodology and the adopted data are described in section 2. Then, the experimental results of both the electrical and thermal models with the predicted efficiencies using the ANN are presented in section 3. Finally, some conclusions are provided in section 4.

2. Methodology and data

The main objective of this study is to present both thermal and electrical modeling process and successively to implement an Artificial Neural Network model, which is able to forecast the electrical and thermal efficiencies of air collector PVT systems. Then, real climatic data of one year are used as an input of the electrical and thermal models to compute corresponding efficiencies. These latter are adopted in the training and validation of the proposed ANN and LS-SVM models.

2.1. PVT air collector modeling

The modeling procedure represents an important task to imitate the real electrical and thermal behaviors of PVT systems. Accordingly, two validated modelling techniques are developed to assess the electrical and thermal performances of the air collector PVT system.

2.1.1. Electrical modeling

Photovoltaic module is a group of cells connected in series to provide important levels of voltage and current, which vary according to the fluctuations of solar irradiance G and cell temperature T_c (Chaibi et al., 2019a). The electrical behavior of PV modules is represented by the equivalent-circuit models. In **Fig.1**, one of the most adopted configurations is presented, noted as the single-diode presentation. Here, two resistances called the shunt R_{sh} and the series resistance R_s are added to take in account the PV cell losses (Chaibi et al., 2018).

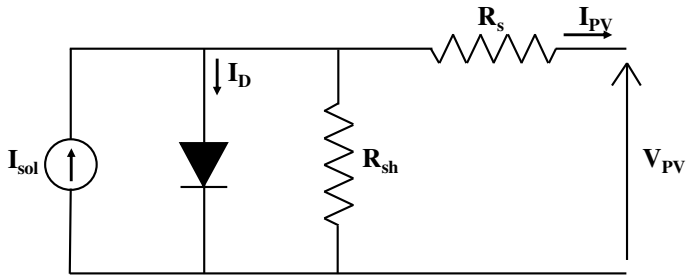

Fig.1: PV cell single-diode equivalent circuit model

The model in **Fig.1** is employed to plot the current-voltage characteristics (I-V). The PV module output current I_{pv} is defined as follows (Villalva et al., 2009):

$$I_{PV} = I_{sol} - I_s\left\{\exp\left[\frac{q}{aN_cKT}(V_{PV} + I_{PV}R_s) - 1\right]\right\} - \frac{V_{PV}+R_sI_{PV}}{R_{sh}} \quad \textbf{(1)}$$

where:

a: diode ideality factor.

I_s: saturation current of the PV module.

I_{sol}: photo-generated current of the PV module.

K: Boltzmann constant.

N_c: number of cells in series.

q: electron charge.

V_{PV}: output voltage of the PV module.

From **Eq.(1)**, the I-V curves nonlinearity could be assessed using the manufacturer datasheet and a numerical process to determine the unknown electrical parameters. An iterative process to extract the equivalent-circuit physical parameters is adopted (Chaibi et al., 2020). This

158 method is based on the iteration of the shunt resistance until finding a good matching between
159 computed and experimental power at the standard test conditions (STC).
160 In order to compute the corresponding powers for each value of solar irradiance and
161 temperature, **Eq.(2)** is used together with **Eq.(1)** to find the maximum power point (MPP)
162 coordinates.

163 $$\frac{\partial P_{PV}}{\partial V_{PV}} = I_{PV} + V_{PV}\frac{\partial I_{PV}}{\partial V_{PV}} = 0 \Rightarrow I_{PV} = (V_{PV} - R_s I_{PV})\left\{\frac{q}{aN_c kT} I_s \exp\left[\frac{q}{aN_c kT}(V_{PV} + R_s I_{PV})\right] +\right.$$

164 $$\left.{}^{1}/_{R_{sh}}\right\} \quad \textbf{(2)}$$

165 Computed powers at MPP are provided to calculate the electrical module efficiency using the
166 following equation (Chaibi et al., 2019b):

167 $$\eta_{ele} = \frac{P_{pv}}{S_m G} \quad \textbf{(3)}$$

168 S_m is the module surface.

169 **2.1.2.** Thermal modeling

170 **Fig.2** depicts the PVT hybrid collector scheme considered in this work. It is constituted
171 of a photovoltaic module with three layers: tempered glass, PV cells covered by two-ethylene
172 vinyl acetate (EVA) layers and Tedlar (Sarhaddi et al., 2010a).

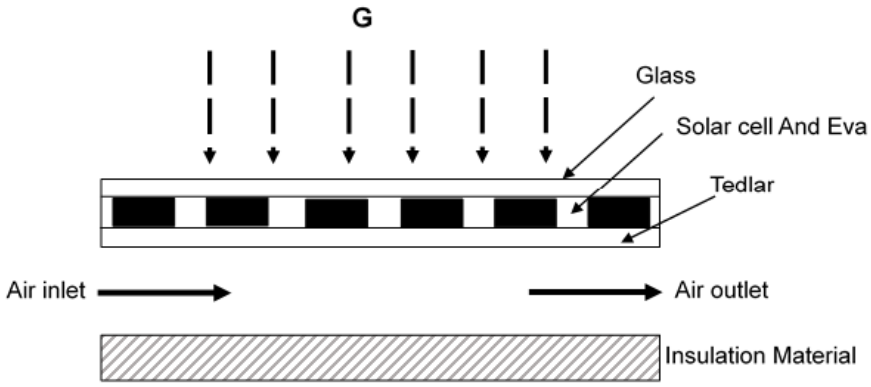

173
174 **Fig.2:** A cross-section picture of a PV/T air module

175 To perform the energy balance for each layer of the PVT module, various assumptions have
176 been applied:

177 - unsteady state conditions;
178 - air is an incompressible fluid;
179 - EVA has a transmissivity of approximately 100%;
180 - temperature of glass, cell, tedlar and air depends only on the longitudinal dimension in
181 the flow direction;

- heat loss is neglected as we consider the PV module to be well insulated.

Fig.3 presents the corresponding equivalent thermal resistance circuit and the size of the control volume for airflow.

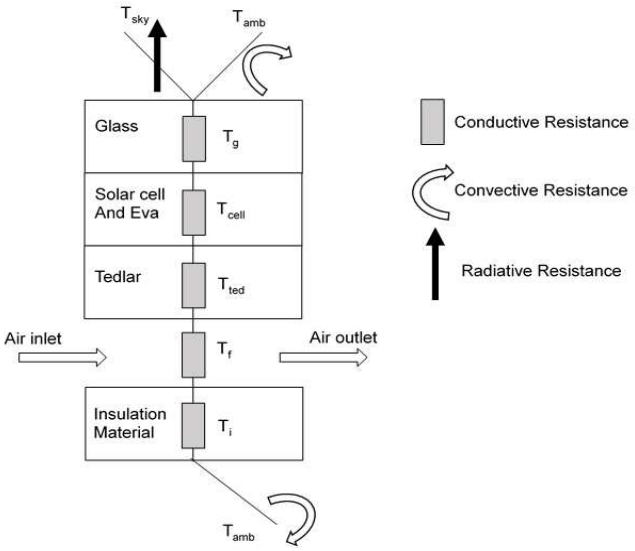

(a)

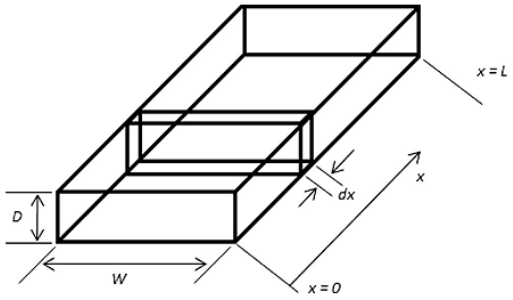

(b)

Fig.3: Layout of thermal resistance system of a PVT air module **(a)**, and basic length "dx" of a control volume **(b)** (Sarhaddi et al., 2010b)

The thermal energy equations for various layers of the system are as follows:

- *Energy equation for glass*

$$(\rho c \delta)_g \frac{\partial T_g}{\partial t} = \lambda_g \delta_g \frac{\partial^2 T_g}{\partial x^2} + \alpha_g G + \sigma \varepsilon_g \left(T_{sky}^4 - T_g^4\right) + h_c \left(T_{am} - T_g\right) + \frac{\lambda_g}{\delta_g}\left(T_c - T_g\right)$$

(4)

where, ρ_g is the density of the glass, c_g is the heat capacity of the glass, δ_g is the thickness of the glass, λ_g is the thermal conductivity of the glass, G is the solar radiation received by the glass, α_g is the absorptivity of the glass, T_{am} is the ambient temperature, σ and ε_g are Stefan

Boltzmann constant and glass emissivity respectively. Swinbank (Sarhaddi et al., 2010a) expression is used to estimate the sky temperature T_{sky}:

$$T_{sky} = 0.0552 T_{am}^{1.5} \quad \textbf{(5)}$$

McAdams correlation is adopted to determine the heat transfer coefficient between air and glass (Swinbank, 1963):

$$h_c = 5.7 + 3.8 V_{wind} \quad \textbf{(6)}$$

where, V_{wind} is the wind speed.

- *Energy equation for PV cell*

$$(\rho c \delta)_c \frac{\partial T_c}{\partial t} = \lambda_c \delta_c \frac{\partial^2 T_c}{\partial x^2} + \left[\frac{\delta_g}{\lambda_g} + \frac{\delta_c}{\lambda_c}\right]^{-1} \left(T_g - T_c\right) + \left[\frac{\delta_{ted}}{\lambda_{ted}} + \frac{\delta_c}{\lambda_c}\right]^{-1} \left(T_{ted} - T_c\right) + G \beta_c \tau_g \alpha_{pv} - P_{pv} \quad \textbf{(7)}$$

The electricity produced by PV cell P_{pv} can be calculated using the following expression (Sellami et al., 2019)**:**

$$P_{pv} = \tau_g \beta_c G \eta_o \left[1 - \beta \left(T_c - T_{ref}\right)\right] \quad \textbf{(8)}$$

where, β is the cell temperature coefficient, β_c is the packing factor, τ_g is the glass transmittance, α_{pv} is the absorptivity of the PV cells and η_o is the reference electrical efficiency of PV panel for a reference temperature T_{ref}.

- *Energy equation for Tedlar*

$$(\rho c \delta)_{ted} \frac{\partial T_{ted}}{\partial t} = \lambda_{ted} \delta_{ted} \frac{\partial^2 T_{ted}}{\partial x^2} + h_f \left(T_f - T_{ted}\right) + \left[\frac{\delta_{ted}}{\lambda_{ted}} + \frac{\delta_c}{\lambda_c}\right]^{-1} \left(T_c - T_{ted}\right) \quad \textbf{(9)}$$

- *Energy equation for air*

$$(\rho c A)_f \frac{\partial T_f}{\partial t} + c_f \dot{m}_f \frac{\partial T_f}{\partial x} = \lambda_f A_f \frac{\partial^2 T_f}{\partial x^2} + h_f . W \left(T_{ted} - T_f\right) \quad \textbf{(10)}$$

where, $\dot{m}_f$ is the mass flow rate of air and A_f is the cross-sectional area of the fluid and W is the PVT width.

The thermal (η_{th}) and electrical efficiency (η_{ele}) are calculated as (Evans, 1981):

$$\eta_{th} = \frac{\dot{m}_f c_f \left(\bar{T}_f - T_{f,in}\right)}{G.A_{pv}} \quad \textbf{(11)}$$

$$\eta_{ele} = \eta_{ref} \beta_c \left(1 - 0.0045\left(\bar{T}_c - 298.15\right)\right) \quad \textbf{(12)}$$

where, $\bar{T}_c$ is the average temperature of the PV cell and $\bar{T}_f$ is the average temperature of the fluid (Rejeb et al., 2020). In this work the reference efficiency η_{ref} is assumed to be 12%, which is in the range of the efficiency of common PV modules (Hazami et al., 2016).

The overall energy efficiency of the PVT module is calculated using the following expression (Good, 2016):

$$\eta_g = \eta_{th} + \frac{\eta_{ele}}{C_F} \quad \textbf{(13)}$$

The electrical energy conversion factor C_F ranges from 0.35 to 0.40 and is generally used for PVT systems (Patankar, 1980).

A fully implicit finite volume method was used to solve the energy equations system. The first-order upwind scheme was applied to address convective terms, and diffusion terms are discretized using the second order of the central differential scheme**.** In this paper, the discretized equations were solved iteratively by using a Tridiagonal Matrix Algorithm (TDMA) method (Patankar, 1980). The computation procedure was carried out using Fortan 90. The specified iteration in each time interval was considered convergent when the maximum relative residual of T_g, T_c, T_{ted} and T_f was less than 10^{-4}.

2.2. Machine learning based methods

This section introduces the supervisor machine learning techniques as the Artificial Neural Network and the Least Squares Support Vector Machines adopted to predict both electrical and thermal performance of a photovoltaic-thermal air collector system.

2.2.1. Artificial Neural Network

Artificial neural network includes an input layer, an output layer and one or more hidden layers. Each layer consists of neurons connected between them. The outputs of each layer are the input for the next layer, get by a transfer (activation) function f as follows:

$$Y_i = f(\sum_j w_j X_i + b) \quad \textbf{(14)}$$

where, Y_i represents the output for the i-th layer based on the input X_i the connection weights w_j and b is the bias (Haykin, 2007). A common scheme of a multi-layer NN is shown in **Fig.4**.

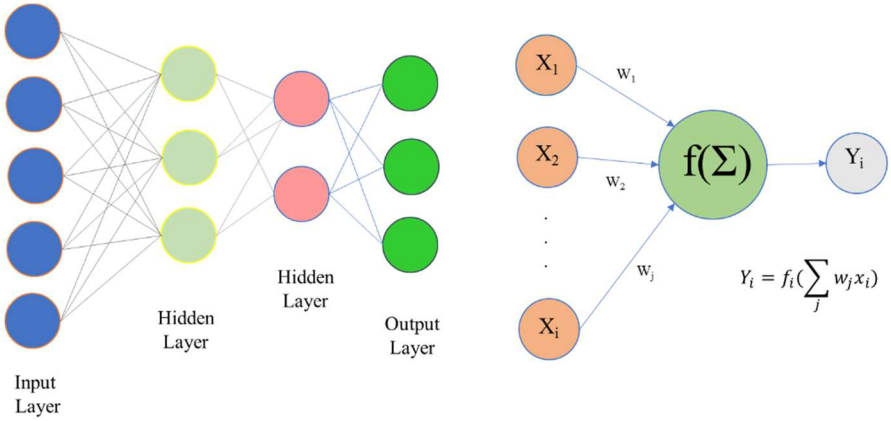

Fig.4: Common multi-layer neural network

The neural networks can be classified into feed-forward and feed-back networks. A feed-forward network is a non-recurrent network where the output is determined by the activation of the neurons starting from input through all the layers in one direction. Unlike a feed-back network can adopt a loop, so the neuron connections can be in more directions (Schmidhuber, 2015).

In common applications, fit a neural network means use a training dataset to set the connection between the neurons (weights) in order to map the inputs and the outputs in the best way possible. So, the training of a feedforward neural network phase consists of an optimization algorithm based on the back-propagation learning algorithm. It includes forward phase and backward phase (De Giorgi et al., 2013). In the Forward phase, the error is obtained as the difference between the target and the actual output with parameters of the network fixed. the Backward phase the weights are adjusted to minimize the error.

The Levenberg–Marquardt algorithm is one of the most popular training algorithm for neural network that adopts the gradient descent approach, by which the training can be considered as completed when the performance is minimized to the goal. A description of the Levenberg-Marquardt algorithm for neural network application can be found (Rojas, 1996).

2.2.2. Least Squares Support Vector Machines

The Least Squares Support Vector Machines represents a noteworthy learning technique with several applications to overcome the overfitting problem successfully. The LS-SVM maps the outputs y_i by using a regression function φ, applied to the inputs x_i as follows:

$$y_i = w\varphi(x_i) + b \quad i = 1 \ldots N \tag{15}$$

where, w is the weight vector, b is the bias and N is the size of the training dataset. The Lagrange function given by:

$$L(w, b, e, \alpha) = \mathcal{J}(w, e) - \sum_{i=1}^{N} \alpha_i \{y_i [w\varphi(x_i) + b] - 1 + e_i\} \quad i = 1 \ldots N \tag{16}$$

It is introduced to solve the optimization problem and to minimize the cost function.

$$\min_{w,e} \mathcal{J}(w, e) = \frac{1}{2} w^T w + \frac{\gamma}{2} \sum_i^N {e_i}^2 \quad i = 1 \ldots N \tag{17}$$

With e_i and α_i are unknown variables and γ is the regularization factor. The Mercer's theorem introduces a kernel function K and claims that:

$$\varphi^T(x_i)\varphi(x_j) = K(x_i, x_j) \quad i, j = 1 \ldots N \tag{18}$$

It assumes the Radial Basis Function (RBF) as the kernel function given by:

$$K(x_k, x_j) = \exp\left(-\frac{\|x_k - x_j\|_2^2}{\sigma^2}\right) \tag{19}$$

with σ the tuning parameter. So, an approximation of y is given by:

$$y(x) = \sum_{i=1}^{N} \alpha_i K(x, x_i) + b \tag{20}$$

2.3.3 Accuracy assessment

The performance of the prediction models is evaluated by:

- P*earson correlation coefficient (R)*

$$R = \frac{n \sum_1^n (x_i * \hat{x}_i) - (\sum_1^n (x_i) * \sum_1^n (\hat{x}_i))}{\sqrt{(n \sum_1^n {x_i}^2 - (\sum_1^n x_i)^2) * (n \sum_1^n {\hat{x}_i}^2 - (\sum_1^n \hat{x}_i)^2)}} \tag{21}$$

- *Root Mean Square Error (RMSE)*

$$RMSE = \sqrt{\frac{1}{n} \cdot \sum_1^n (x_i - \hat{x}_i)^2} \tag{22}$$

- *Mean absolute Error (MAE)*

$$MAE = \frac{1}{n} \cdot \sum_1^n (x_i - \hat{x}_i) \tag{23}$$

with $\hat{x}_i$ outputs, x_i targets and n is the size of the testing dataset. Low MAE implies good fitting between actual outputs and targets. R value is closed to 1 mean a good relationship among actual data and predicted one.

3. Results and discussion

In this section, the experimental validation of both electrical and thermal models is assessed. Then, the obtained results of the ANN-based model are presented and compared to the
LS-SVM model.

3.1. Data description

In this study, the input climatic data (Dalala et al., 2020) are the real measurements of solar irradiance, module temperature, humidity and wind recorded in a weather station located at Jordan valley site (Hashemite Kingdome of Jordan) for the 2017 year. More details are reported in (Dalala et al., 2020). The monitored data every 30 minutes, for 12.238 samples overall, are used as input of the developed electrical and thermal models. The test dataset of 3456 samples are plotted in **Fig.5**.

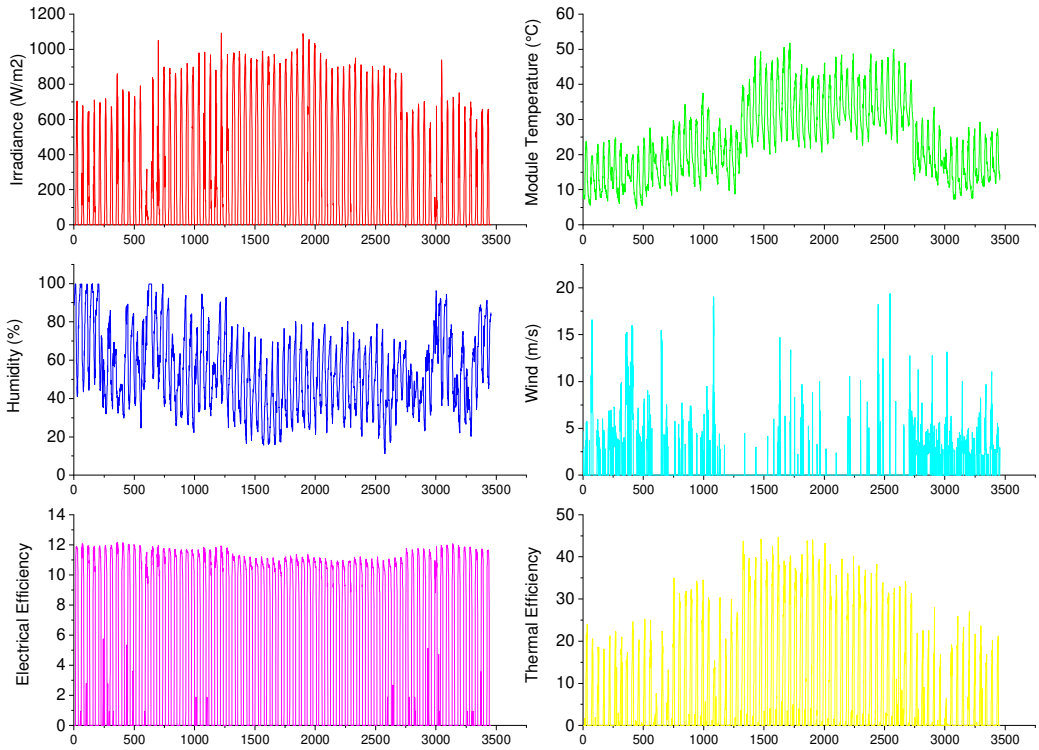

Fig.5: Test weather data and efficiency related to 2017 year.

The horizontal solar irradiance varies between 0 and 1093.06 W/m^2 with the mean value is 229.52 W/m^2. The module temperature is in the range 4.72 °C ÷ 51.82 °C with the lowest value in January, the highest value in June and a mean value of 24.13°C. The humidity is 11.33% in September, 99.81% in March and 54.12% on annual average. The highest wind value is recorded of 19.4 m/s with a mean of 1.1 m/s. The highest electrical and thermal

efficiencies are 12.7% in January and 44.66% in June with a mean of 5.27% and 6.98% respectively.

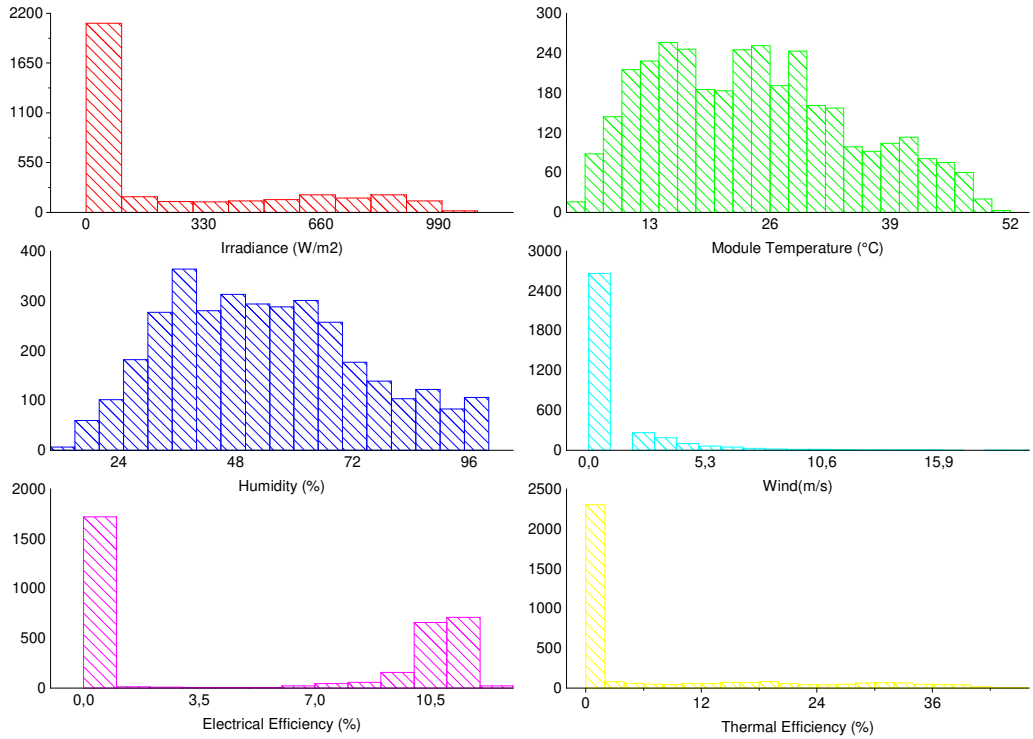

Fig.6: Variables Distribution Histograms

The distribution histograms of the used data are plotted in **Fig.6**. The solar irradiance and the wind show a distribution that "leans" to the left (positive skewness) that means the lack of symmetry with respect to the mean, unlike by the module temperature and humidity which present a distribution similar to the uniform one. It is noted that the electrical and thermal efficiencies show the same distribution as the solar irradiance and wind.

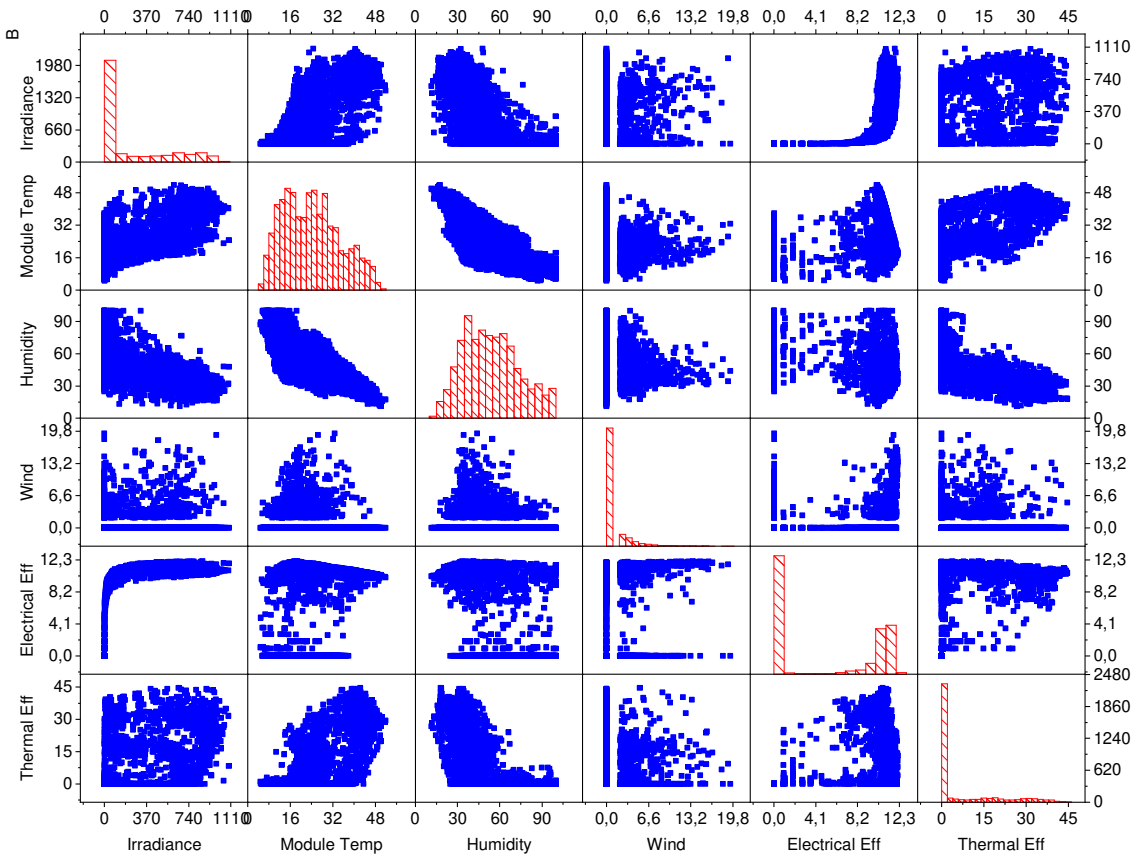

Fig.7: Scatter matrix of the variables

The **Fig.7** shows the correlation between the input climatic data and the efficiencies (electrical and thermal). In very few cases it is possible to see a correlation between the variables. An increase/decrease pattern exists between irradiance, module temperature, electrical and thermal efficiency.

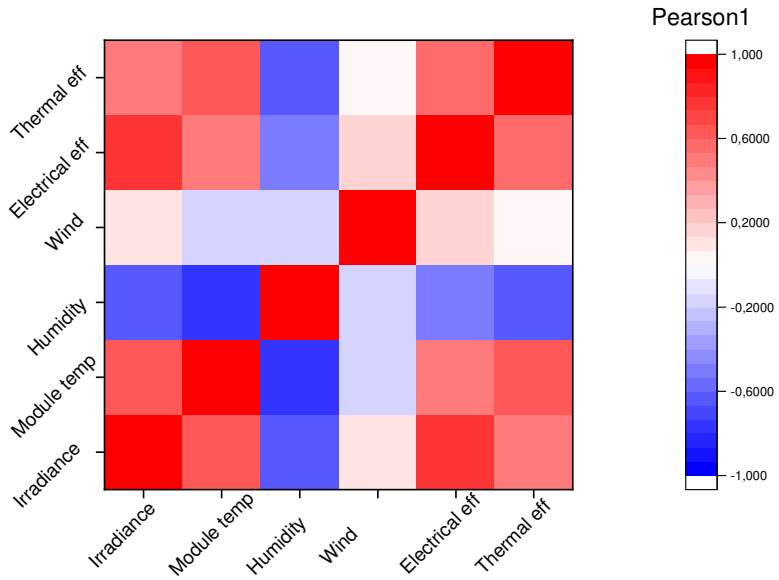

Fig.8: Pearson Correlation Coefficients

In fact, as shown in **Fig. 8**, the Pearson correlation coefficient is close to 1, or however higher than 0.6 in very few cases. Sometimes we can see also negative correlations. The electrical and thermal efficiencies present a correlation of 0.78 and 0.53 with irradiance respectively; of 0.49 and 0.62 with the module temperature. The remain variables such as humidity and wind show a correlation very closed to 0 or even negative correlation.

Such analysis will be considered in the development of the ANN model. In particular, the correlations will represent the criteria by which the variables will be chosen as input for the ANN.

3.2. Validation of the electrical and thermal models

3.2.1. Electrical model

To assess the accuracy of the electrical PV modeling, datasheet values of the SP75 PV module (See **Table 1**) are used to compute the electrical parameters using the iterative process reported in (Chaibi et al., 2020). The founded parameters are summarized in **Table 2**.

Table. 1: Specifications of the used PVT air collector system (Sarhaddi et al., 2010a)

Solar PVT air module parameters	**Value**
PV module type	Siemens SP75, monocrystalline silicon
The number of cells in series, N_c	36
The maximum power of PV module at STC, $P_{pv,MPP}$	75 W
The maximum voltage of PV module at STC, $V_{pv,MPP}$	17 V
The maximum current of PV module at STC, $I_{pv,MPP}$	4.4 A
The short-circuit current of PV module at STC, I_{sc}	4.8 A
The open-circuit voltage of PV module at STC,V_{oc}	21.7 V
The temperature coefficient of I_{sc}, K_i	2.06 mA/°C
The length of PV module, L	1.2 m
The width of PV module, W	0.527 m
The area of PV module, S_m	0.632 m^2
The electrical efficiency at the reference conditions, $\eta_{ele,ref}$	0.12
The density of glass cover, ρ_g	2450 $kg.m^{-3}$
The specific heat capacity of glass cover, c_g	500 $J.kg^{-1}.K^{-1}$
The thickness of glass cover, δ_g	0.003 m
The conductivity of glass cover, λ_g	1 $W.m^{-1}.K^{-1}$
The transmissivity of glass cover, τ_g	0.95
The conductivity of solar cell, λ_c	130 $W.m^{-1}.K^{-1}$
The specific heat capacity of solar cell, c_c	677 $J.kg^{-1}.K^{-1}$
The density of solar cell, ρ_c	2330 $kg.m^{-3}$
The absorptivity of solar cell, α_c	0.85
The thickness of solar cell, δ_c	0.0003 m

The conductivity of solar cell, λ_c	0.036 W. m^{-1}.K^{-1}
The thickness of tedlar, δ_{ted}	0.0005 m
The conductivity of tedlar, λ_{ted}	0.033 W. m^{-1}.K^{-1}
The specific heat capacity of tedlar, c_{ted}	1250 J.kg^{-1}.K^{-1}
The density of tedlar, ρ_{ted}	1200 kg.m^{-3}

Table. 2: Extracted parameters of the Siemens SP75 PV module at the STC (Chaibi et al., 2020)

Parameters	Value
Photo-generated current	4.8 A
Saturation current	1.1e-06 A
Ideality factor	1.5352
Series resistance	0.2616 Ω
Shunt resistance	2670 Ω

The parameters in **Table 2** are adopted to generate the I-V curves of the SP75 PV module. Then, these characteristics are compared to the experimental curves for various level of solar irradiance and temperature. These I-V curves are presented in **Fig.9**, with a variation of solar irradiance and fixed temperature at 25 °C (**Fig.9-a**), and variation of temperature with a fixed irradiance at 1000 W/m^2 (**Fig.9-b**). It is clear from these curves that the adopted modeling method exhibits high accuracy for different variations of solar irradiance and temperature. Besides, a little disagreement is remarked for irradiances below 400 W/m^2, but it will not affect the performances of the electrical model since it does not exceed 2% of difference compared to experimental data.

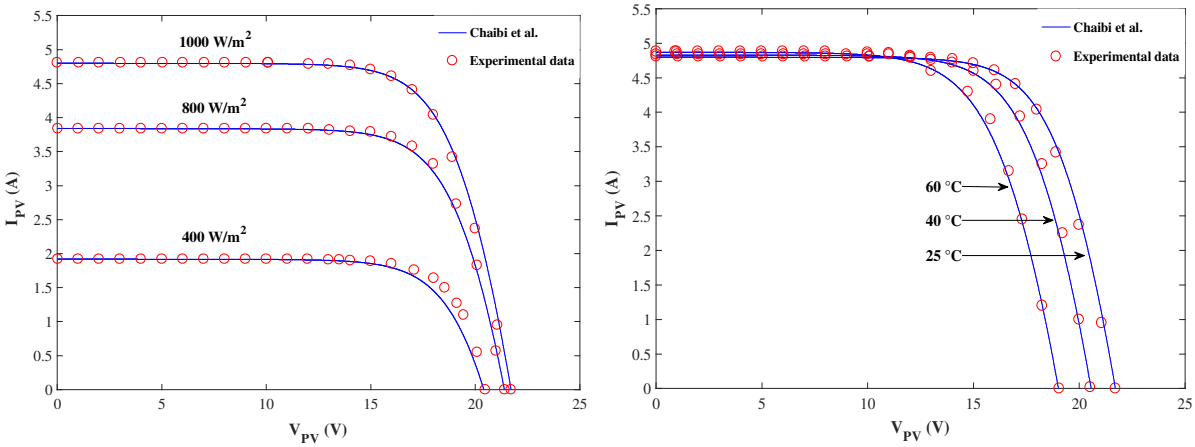

(a) **(b)**

Fig.9: Experimental and simulated I-V characteristics of the SP75 PV module: irradiance varies and fixed temperature (T=25°C) **(a)**, temperature varies and fixed irradiance (G=1000 W/m^2) **(b)**

3.2.2. Thermal model

Numerical results obtained by the thermal model are compared to the experimental results reported by Joshi et al. (Joshi et al., 2009). Solar irradiance, ambient temperature, air temperature at the inlet and outlet of the PVT, and PV cell temperature are some of the parameters that Joshi et al. (Joshi et al., 2009) have measured. The design parameters and thermophysical properties of the PVT air collector are presented in **Table 1** (Sarhaddi et al., 2010a). **Fig.10** indicates the experimental day's variations in solar radiation intensity, ambient temperature and inlet air temperature. **Fig.11** illustrates the variation versus time of the air temperature at the output of the PVT module, the average PV cell temperature and the related experimental data. Based on this figure, there is generally a good correspondence between experimental and numerical results. The thermal and electrical efficiencies of the PVT air system are illustrated in **Fig.12.** Here, it can be seen that there is a reasonable agreement between experimental and calculated values of these efficiencies. The slight difference between the experimental and calculated efficiencies can be explained as follows:

- Wind speed is considered constant. However, in practice this velocity is not constant and has a direct effect on the heat loss through the system;
- The absorption and transmission coefficients were considered constant while they vary over the day as solar incidence angle on the PVT system surface changes.

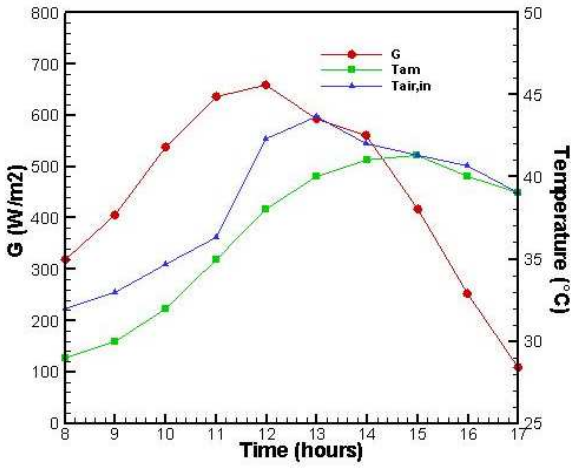

Fig.10: The hourly variation of G, T_{am} and $T_{air,inlet}$

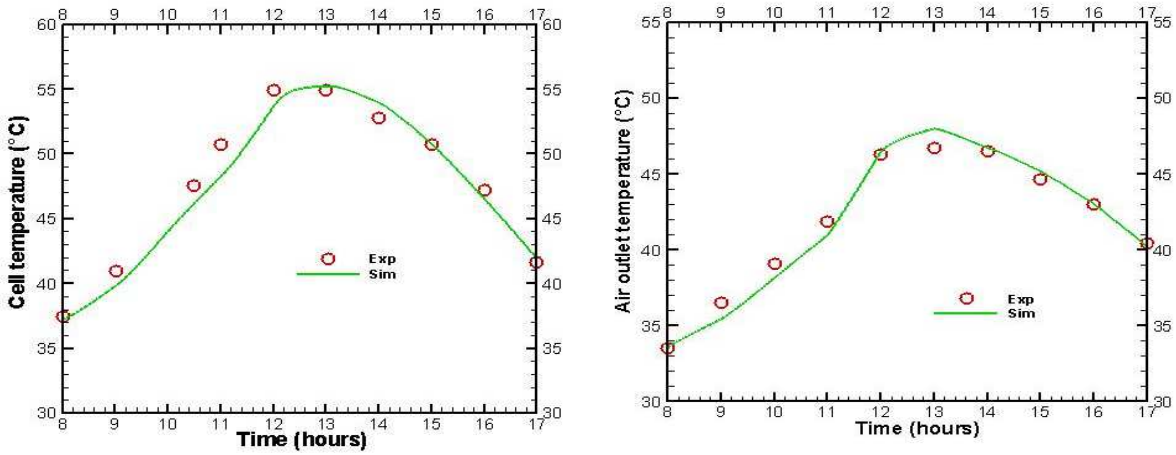

(a) (b)

Fig.11: Numerical and experimental results: Outlet air temperature **(a)**, and average cell temperature **(b)**

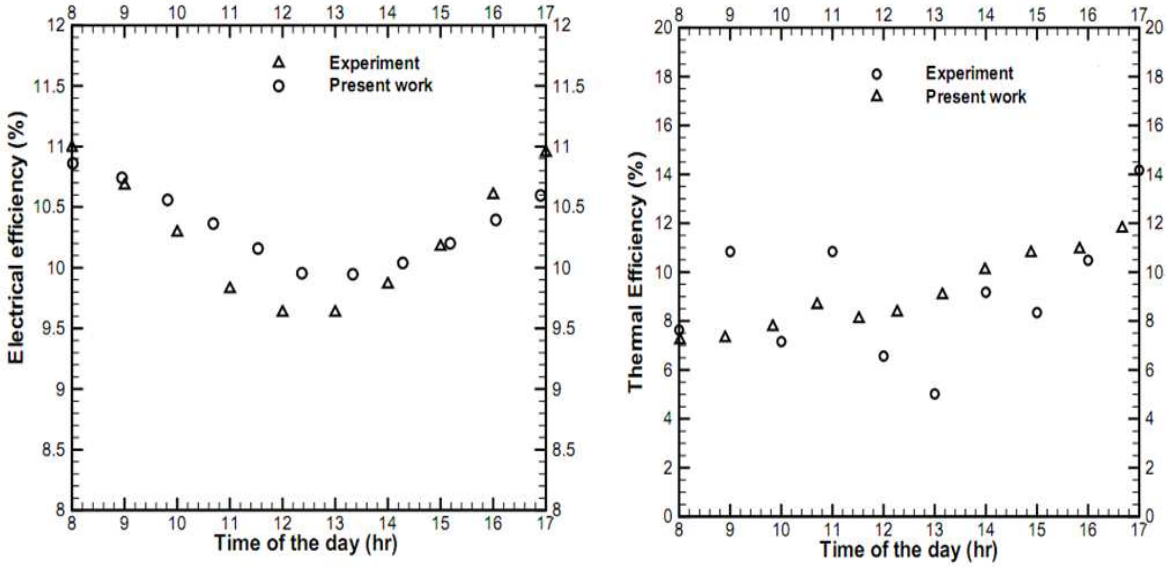

(a) (b)

Fig.12: Efficiencies of the PV/T air versus time: Electrical efficiency **(a),** and thermal efficiency (**b)**

3.3. ANN-based model results

In the present work a Multilayer Perceptron (MLP) feedforward neural network of 4 layers is design with 1 input node and 1 output neuron, 1 hidden layers 10 nodes and 1 output layer. The two-layer feedforward network consists of sigmoid hidden neurons and linear output neurons as shown in **Fig.13**.

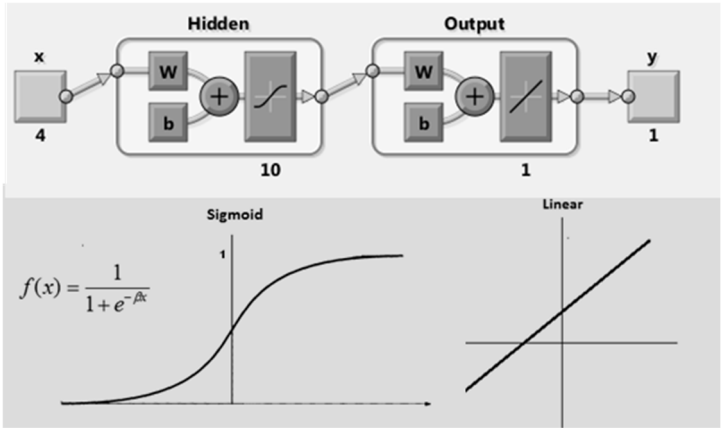

Fig.13: Network Architecture

The sigmoid function used in the ANN hidden layer is defined as (Kang, 2017):

$$f(x) = \frac{1}{1+ e^{-\beta x}} \quad \textbf{(24)}$$

The linear function is given by:

$$g(x) = ax + b \quad \textbf{(25)}$$

They are shown in **Fig.13**. The MLP feedforward neural network implements the Back-Propagation (BP) learning in Batch mode during the BP training, in which the weights are adjusted through epoch-by-epoch that means, the whole dataset is use to training.

The **Table. 3** includes several combinations of the weather variables as the potential input of the neural network. They were chosen on the base of the results regarding the Pearson Correlation Coefficients. So, the variables which exhibited high correlations with the output variables (electrical and thermal efficiencies) were considered to define the cases as presented in the **Table 3**. Further, 2 combinations (case 6 and case 8) of the input variables with low correlations were also considered to analyze their impact on the neural network performance.

Table. 3: Several combinations of the weather variables as the potential input of the neural network

	Solar Irradiance	**Module Temperature**	**Humidity**	**Wind**
Case 1	√	√	√	√
Case 2	√			
Case 3	√	√		
Case 4	√	√		√
Case 5	√	√	√	
Case 6		√	√	√
Case 7	√			√

Case 8		√	√	

For each case, different neural networks were trained and tested by varying the number of hidden layer neurons. The RMSE as defined by **Eq.(22)** is used to assess the performance of the network. The number of hidden layer neurons with lower RMSE was chosen to get the network with higher performance. **Fig. 14** shows the performance in term of RMSEs related to neural networks implemented to predict the electrical and thermal efficiencies respectively for each case. Steady RMSEs were observed within 30 as number of hidden layer neurons. This was established as the maximum number of hidden layer neurons to apply in the performance assessment.

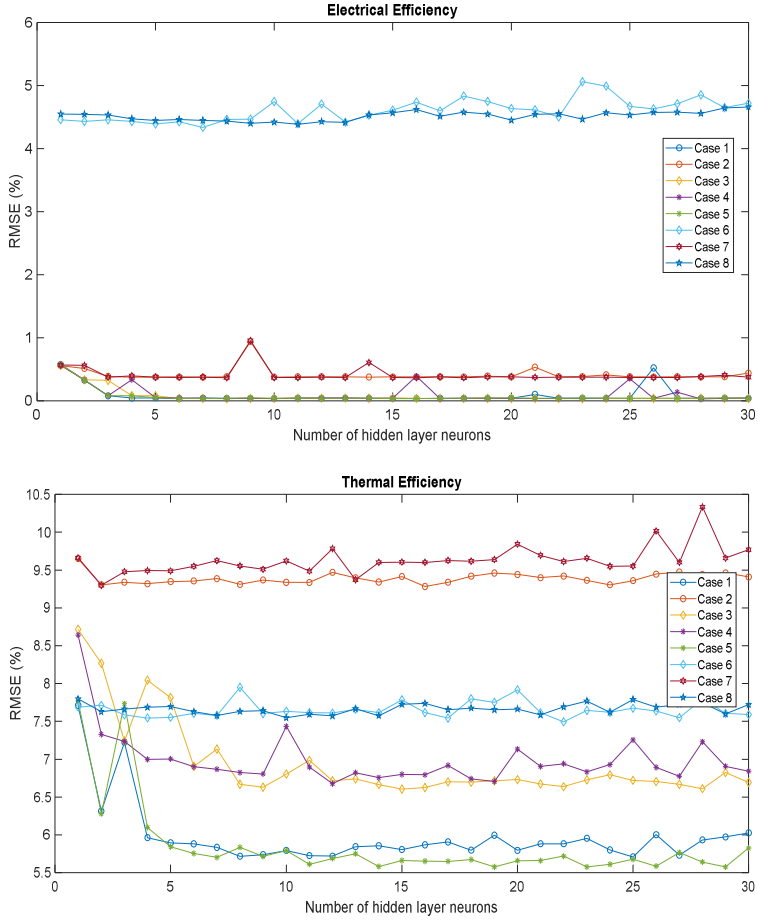

Fig.14: Performance of different neural networks by varying the number of hidden layer neurons

In **Fig 14**, it is clear that the RMSE related to the electric efficiency is lower than 1% excepted for case 6 and 8 in which it varies between 4% and 5%. The case 3 and 5 result more performing with a number of hidden layer neurons starting from 6. The RMSEs of the thermal efficiency are in the range [5.5%, 10.5%]. The best and the worst perform were for the case 5 and the case 7 respectively.

Table 4: Summary of number of hidden layer neurons and R for 8 cases

	Electrical Efficiency		Thermal Efficiency	
	Number of hidden layer neurons	R	Number of hidden layer neurons	R
Case 1	6	0.99998	25	0.85879
Case 2	7	0.99699	16	0.61297
Case 3	8	0.99998	15	0.82186
Case 4	28	0.99997	12	0.81293
Case 5	16	0.99997	29	0.86836
Case 6	7	0.51172	22	0.76551
Case 7	18	0.99783	2	0.58601
Case 8	11	0.51186	10	0.75414

The best number of hidden layer neurons for each case is summarized in **Table 4**. Generally, it can be observed that the neural network to predict the electrical efficiency performs well for low number of hidden layer neurons, unlike the neural network to model the thermal efficiency that shows high accuracy for high number of hidden layer neurons. The best number of hidden layer neurons for each case were adopted for the performance assessment in the following sections.

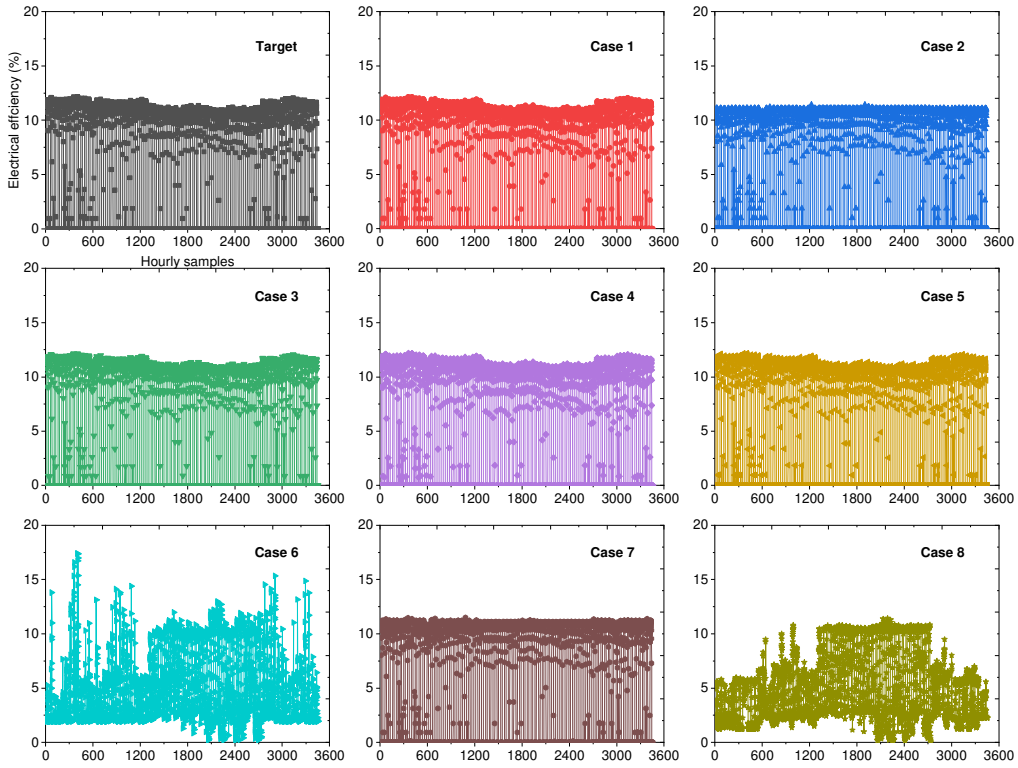

Fig.15: Target VS predicted values of the electrical efficiency.

Fig.15 plots the actual values (target) and the predicted values of the electrical efficiency. For each case, the neural network's response is quite similar to the expected value, excepted for case 6 and 8 which represent the weather variables combinations without the solar irradiance.

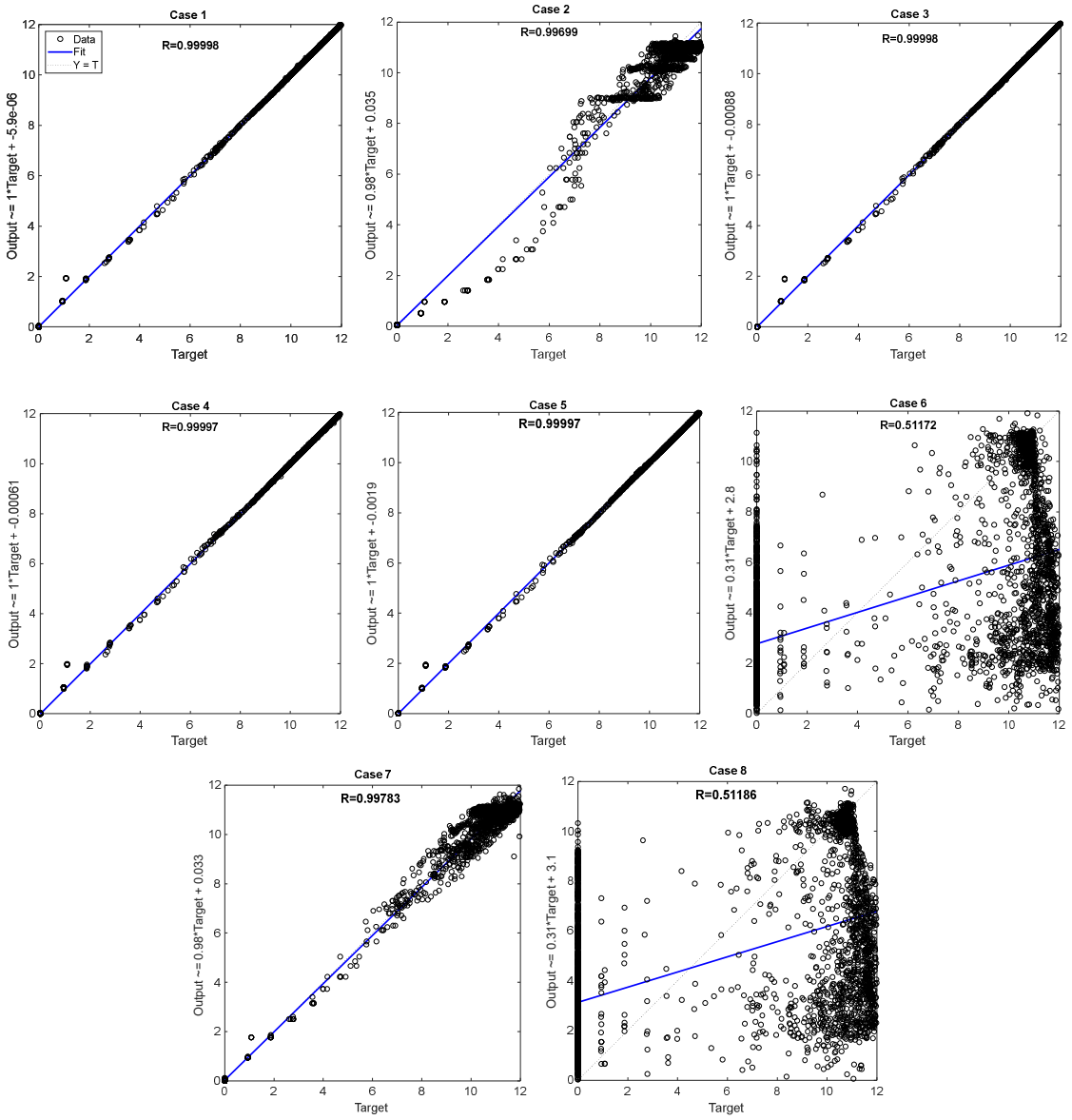

Fig.16: Regression plot for electrical efficiency

Fig. 16 presents regression plots for electrical efficiency. Mainly the R value is 0.99 excepted 0.51 for case 6 and 8.

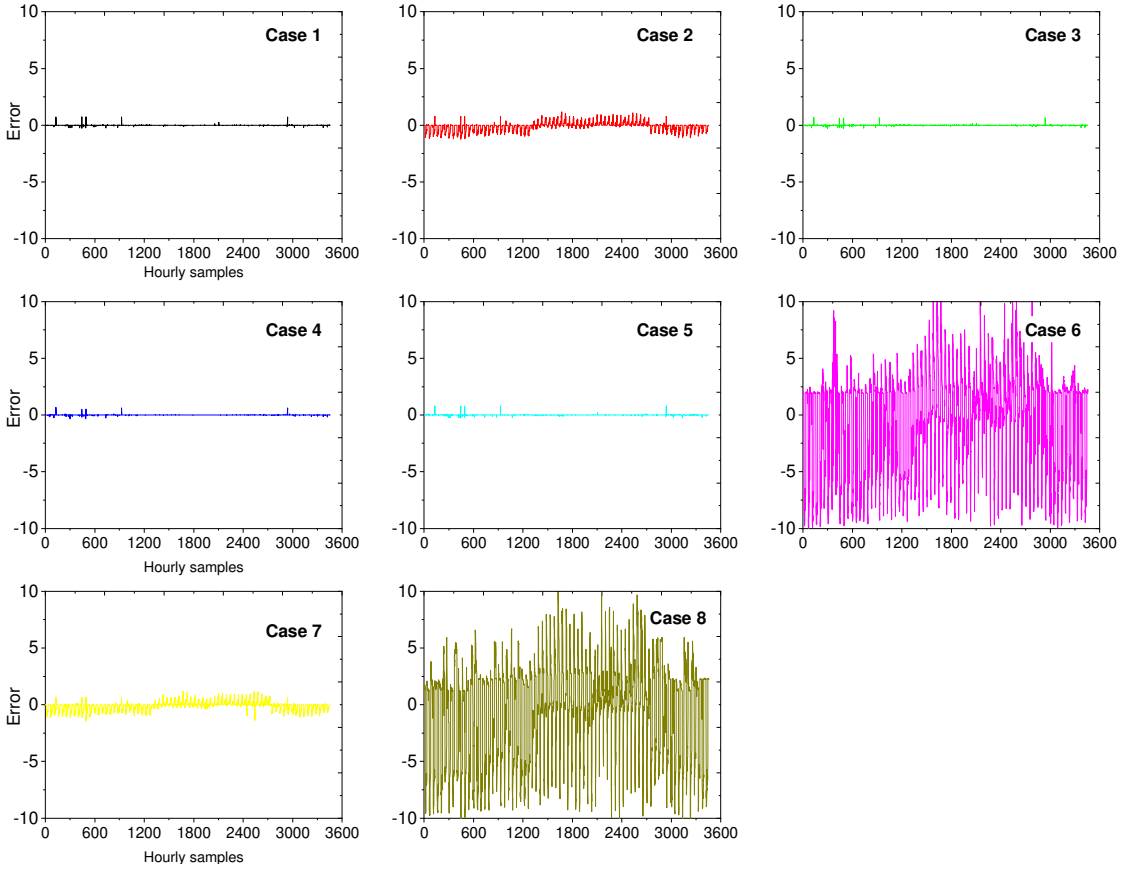

Fig.17: Electrical efficiency error

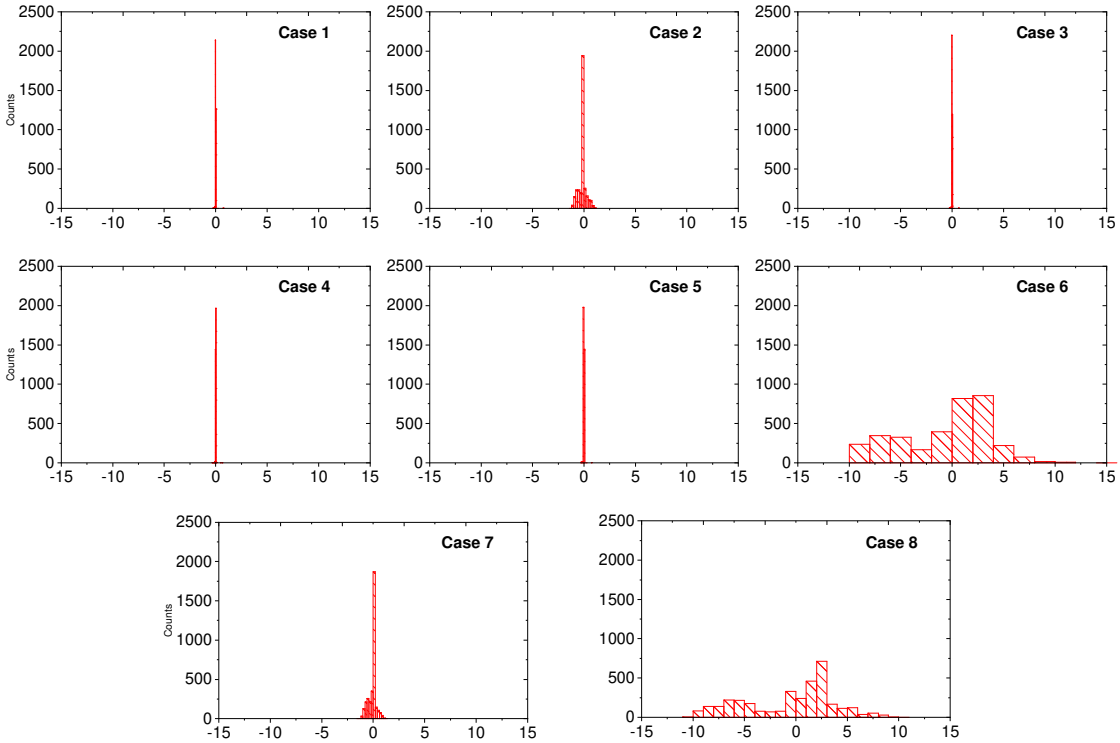

Fig.18: Electrical efficiency error histograms

In **Fig. 17** the errors generally are very low, exhibiting good compliance between target and output, but evident spikes can be observed between -10% and 10% in case 6 and 8. In fact the error histograms (**Fig. 18**) demonstrate that the error distribution is mainly peaked and centered to zero, unlike it is flat for case 6 and it is very flat for case 8.

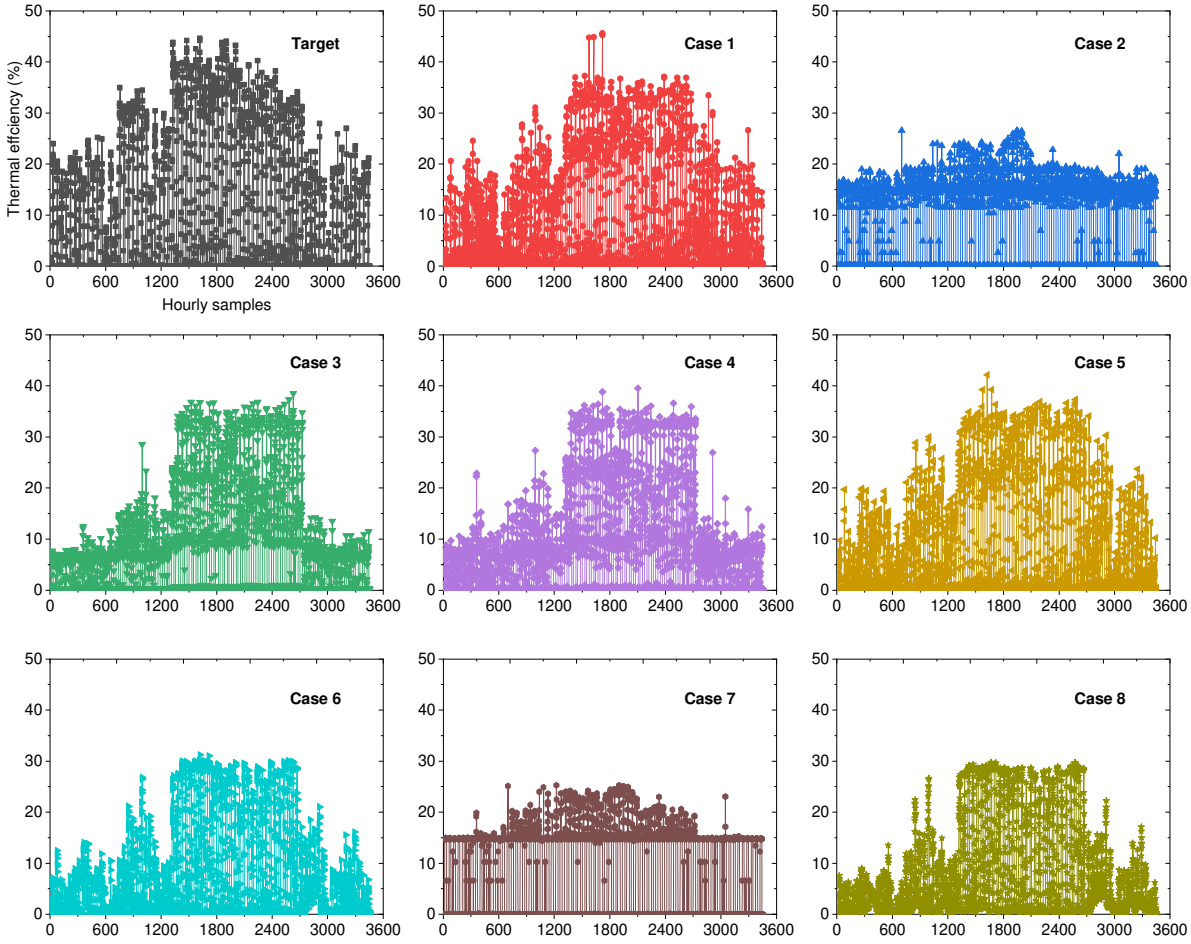

Fig.19: Target and predicted values of the thermal efficiency

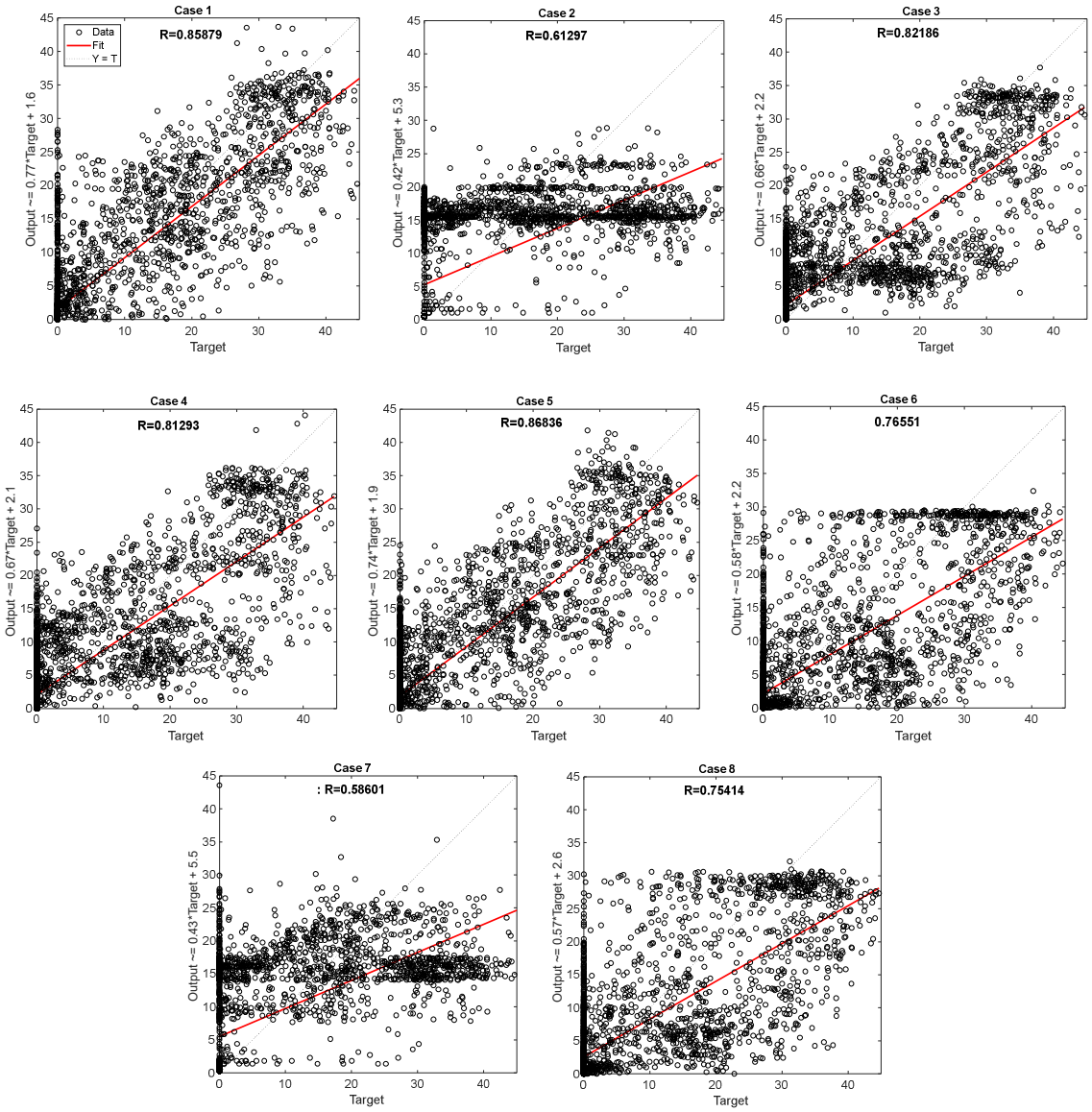

Fig.20: Regression plot for thermal efficiency

The target and the predicted value of the thermal efficiency are presented in **Fig.19**. The implemented neural networks show different responses of the thermal efficiency for the 8 cases. The regression plots (**Fig.20**) illustrate R values up to 0.86 (case 5) and 0.85 (case 1). The worst R value (0.58) is for case 7 that does not consider the module temperature as input of the neural network (see **Table 3**).

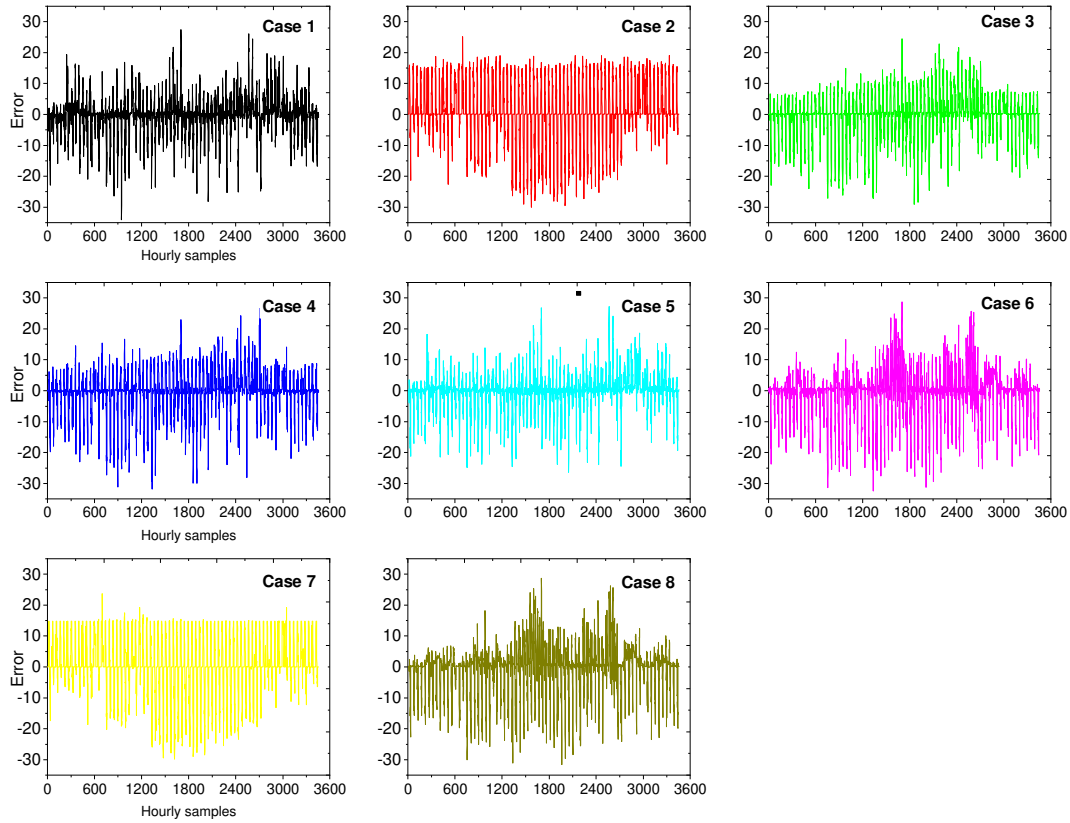

Fig.21: Thermal efficiency error

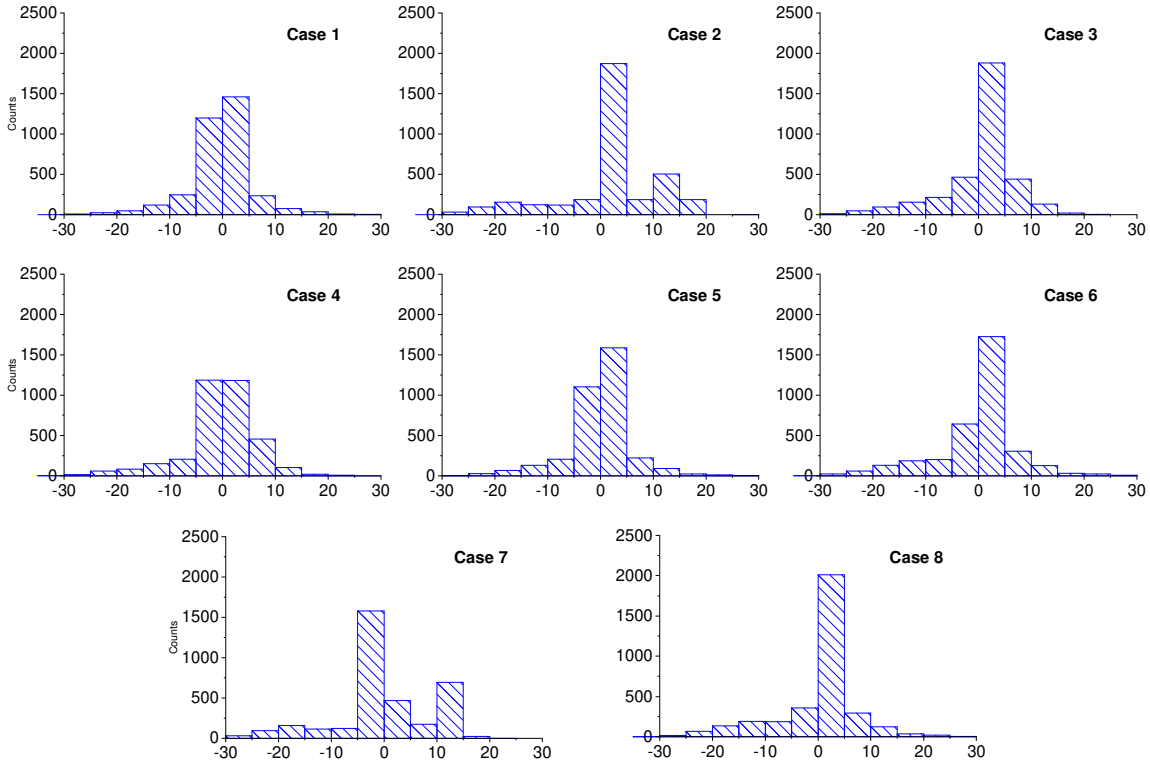

Fig.22: Thermal efficiency error histograms

Fig.21 depicts the errors and confirms that the case 7 presents low error, the remain cases are affected by evident spikes. The thermal efficiency error histograms (**Fig.22**) are left shift: This means that it is more probable to underestimate the thermal efficiency than to overestimate it. Furthermore, the histograms are low with not evident peaks, so positive and negative errors occur with comparable probability.

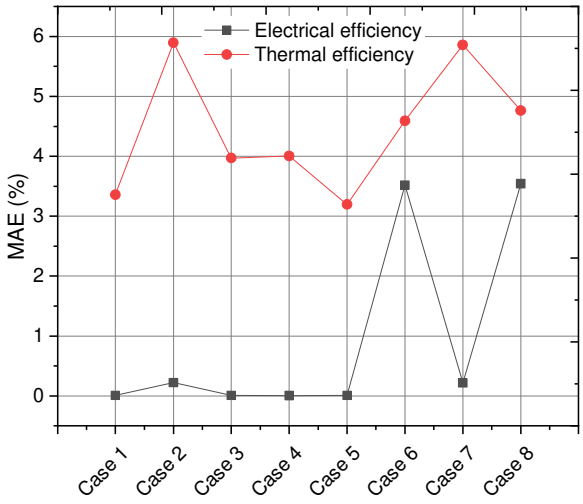

Fig.23: MAE for electrical and thermal efficiency for 8 cases

The MAEs of each case, calculated by **Eq.(23)**, are plotted in **Fig. 23.** Regarding the electrical efficiency, the case 1, 3, 4 and 5 show the best performances in term of MAE closed to zero. For such cases, solar irradiance and module temperature are the common variables, so humidity and wind variables are not essential to obtain high accuracy. High MAEs (up to 3.5%) are remarked in the case 6 and 8 which not consider the solar irradiance as input of the neural network. MAEs of 3.2% can be obtained for thermal efficiency in case 1 and 5 which include the solar irradiance, module temperature and humidity as input. High MAEs (5.9 %) are reported for the cases 2 and 7 which not include module temperature. Such results are in accord with the correlations shown in **Fig.8**, where the electrical efficiency is strictly correlated with the irradiance, the thermal efficiency is correlated with the module temperature.

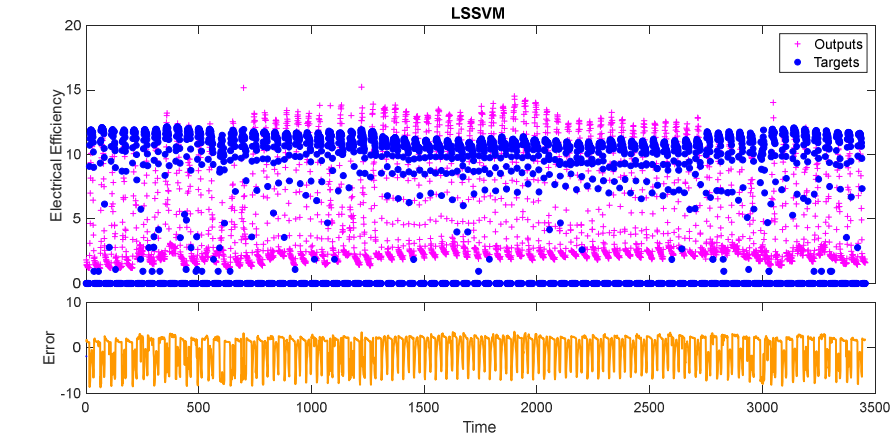

(a)

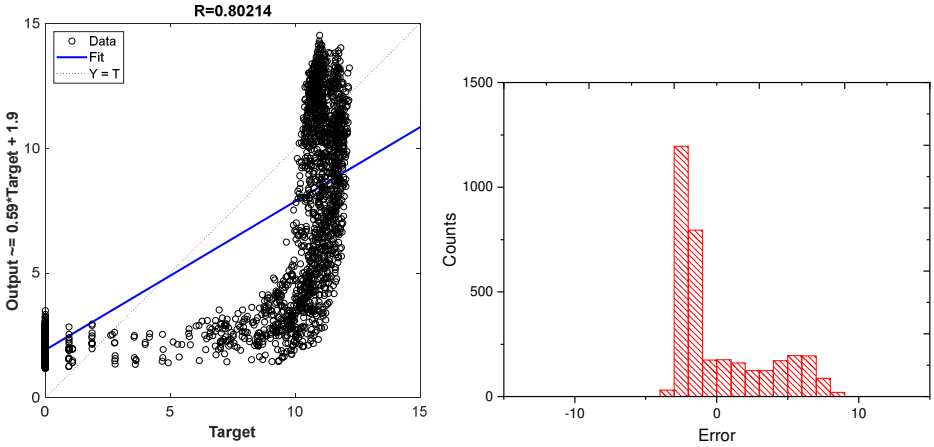

(b) (c)

Fig.24: Actual VS predicted **(a)** R **(b)** and Error histograms **(c)** of the electrical efficiency by LSSVM.

In order to demonstrate the high performance of the discussed neural network-based model, a comparison with the LS-SVM technique is illustrated. Solar irradiance, module temperature, humidity and wind (case 1) were used as input for the LS-SVM model. **Fig.24.a** plot the electrical efficiency targets and outputs. It is evident that the response of the LS-SVM model is very spread if it is compared with the actual electrical efficiency as the R value of 0.80214 confirms (**Fig.24.b**). The error distribution is left shift (**Fig.24.c**) that means most of all the predicted values underestimate the actual electrical efficiency.

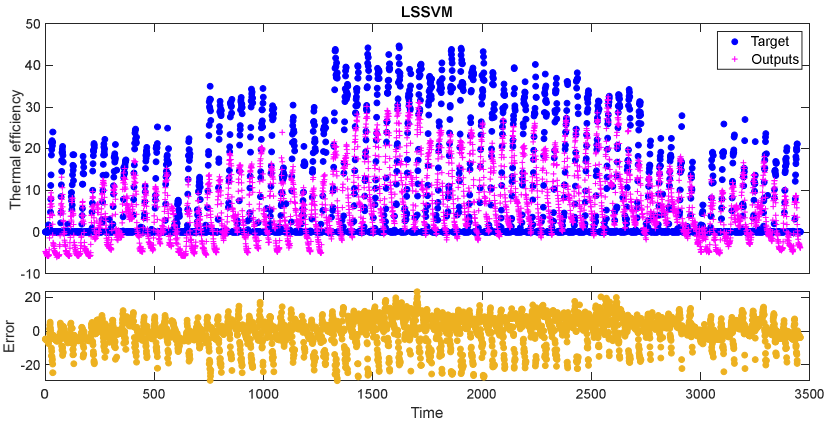

(a)

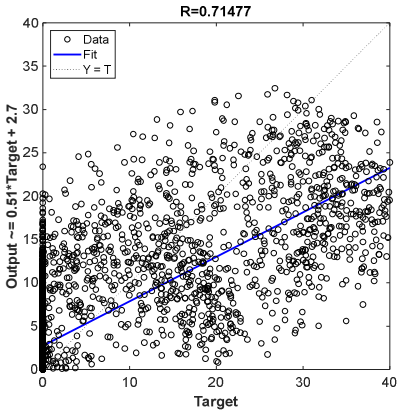

(b)

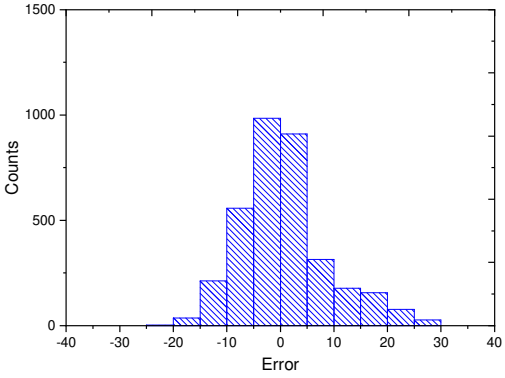

(c)

Fig.25: Actual and predicted values of the thermal efficiency by LS-SVM **(a)** R value **(b)** and Error histograms **(c)** of the thermal efficiency by LS-SVM

The actual and predicted thermal efficiency by LS-SVM is illustrated in **Fig.25.a**. Furthermore, the low R coefficient (0.71477) confirms that exists a not strong correlation (**Fig. 25.b)** and a quite similar probability to underestimate and overestimate the thermal efficiency as seen by the symmetric error distribution (**Fig.25.c**).

Table 5: ANN vs LS-SVM

	ANN		**LS-SVM**	
	Electrical Efficiency	Thermal Efficiency	Electrical Efficiency	Thermal Efficiency
MAE (%)	0.0078	3.3607	2.6936	6.1546

The **Table 5** summarizes the MAE for ANN and LS-SVM using the prediction models for both electrical and thermal efficiency. The results of the case 1 were adopted to compare the performance of the NN-based model. It can see that the ANN outperforms the LS-SVM showing very low MAE values for both efficiencies. The accuracy assessment confirms that the electrical and thermal efficiency of a PVT air system can be predicted with higher

performance by using an ANN than LS-SVM based-model, with a reducing up to 2.7% for electrical efficiency and up to 2.8% for the thermal efficiency.

Conclusion

The study presents the results of an ANN model to predict the electrical and thermal efficiencies of PVT air systems. The first part of the paper introduces a method to model the electrical and the thermal efficiencies. Such method is evaluated by using actual measurements of weather conditions. Then the efficiency modeled values are applied to train and test a predictive model based on ANN using the weather data as an input for the neural networks. Different combinations of the weather variables were considered to assess the performance of the ANN- based model. The results are presented, and an accuracy analysis is performed by RMSE, R coefficient and MAE. The outcomes demonstrate that the choice of the variables as input of the neural network is very important to perform a model with low error. Furthermore, the solar irradiance and the module temperature are the most important variables to consider as input in a NN-based model respectively. The results also demonstrate higher performance of the ANN than LS-SVM. Furthermore, the electrical efficiency can be predicted with higher accuracy than the thermal efficiency.

Funding

The contribution of the School of Electrical and Computer Engineering, National Technical University of Athens was funded by the European Union's Horizon 2020 research and innovation programme under the Marie Skłodowska-Curie grant agreement No 799835.

References

Abdelrazik, A.S., Al-Sulaiman, F.A., Saidur, R., Ben-Mansour, R., 2018. A review on recent development for the design and packaging of hybrid photovoltaic/thermal (PV/T) solar systems. Renew. Sustain. Energy Rev. 95, 110–129. https://doi.org/10.1016/j.rser.2018.07.013

Agrawal, S., Tiwari, G.N., 2013. Overall energy, exergy and carbon credit analysis by different type of hybrid photovoltaic thermal air collectors. Energy Convers. Manag. 65, 628–636. https://doi.org/10.1016/j.enconman.2012.09.020

Ahmadi, M.H., Baghban, A., Salwana, E., Sadeghzadeh, M., Zamen, M., Shamshirband, S., Kumar, R., 2019. Machine Learning Prediction Models of Electrical Efficiency of Photovoltaic-Thermal Collectors. https://doi.org/10.20944/preprints201905.0033.v1

Al Tarabsheh, A., Etier, I., Fath, H., Ghazal, A., Morci, Y., Asad, M., El Haj, A., 2016. Performance of photovoltaic cells in photovoltaic thermal (PVT) modules. IET Renew. Power Gener. 10, 1017–1023. https://doi.org/10.1049/iet-rpg.2016.0001

Babu, C., Ponnambalam, P., 2018. The theoretical performance evaluation of hybrid PV-TEG system. Energy Convers. Manag. 173, 450–460. https://doi.org/10.1016/j.enconman.2018.07.104

Barone, G., Buonomano, A., Forzano, C., Palombo, A., Panagopoulos, O., 2019. Experimentation, modelling and applications of a novel low-cost air-based photovoltaic thermal collector prototype. Energy Convers. Manag. 195, 1079–1097. https://doi.org/10.1016/j.enconman.2019.04.082

Caner, M., Gedik, E., Keĉebaŝ, A., 2011. Investigation on thermal performance calculation of two type solar air collectors using artificial neural network. Expert Syst. Appl. 38, 1668–1674. https://doi.org/10.1016/j.eswa.2010.07.090

Chaibi, Y., Allouhi, A., Malvoni, M., Salhi, M., Saadani, R., 2019a. Solar irradiance and temperature influence on the photovoltaic cell equivalent-circuit models. Sol. Energy 188, 1102–1110. https://doi.org/10.1016/j.solener.2019.07.005

Chaibi, Y., Allouhi, A., Salhi, M., 2020. A simple iterative method to determine the electrical parameters of photovoltaic cell. J. Clean. Prod. 122363. https://doi.org/10.1016/j.jclepro.2020.122363

Chaibi, Y., Allouhi, A., Salhi, M., El-jouni, A., 2019b. Annual performance analysis of different maximum power point tracking techniques used in photovoltaic systems. Prot. Control Mod. Power Syst. 4. https://doi.org/10.1186/s41601-019-0129-1

Chaibi, Y., ElRhafiki, T., Simón-Allué, R., Guedea, I., Luaces, S.C., Gajate, O.C., Kousksou, T., Zeraouli, Y., 2021. Air-based hybrid Photovoltaic/Thermal systems: A review Y. J. Clean. Prod. https://doi.org/10.1016/j.jclepro.2021.126211

Chaibi, Y., Salhi, M., El-jouni, A., Essadki, A., 2018. A new method to extract the equivalent circuit parameters of a photovoltaic panel. Sol. Energy 163, 376–386. https://doi.org/10.1016/j.solener.2018.02.017

Dalala, Z., Al-Addous, M., Alawneh, F., Class, C.B., 2020. Environmental data set for the design and analysis of the Photovoltaic system in the Jordan Valley. Data Br. 31, 105794. https://doi.org/10.1016/j.dib.2020.105794

De Giorgi, M.G., Congedo, P.M., Malvoni, M., Tarantino, M., 2013. Short-term power forecasting by statistical methods for photovoltaic plants in south Italy, in: Proceedings of the Fourth IMEKO TC19 Symposium on Environmental Instrumentation and Measurements: Protection Environment, Climate Changes and Pollution Control. pp. 171–175.

Diwania, S., Agrawal, S., Siddiqui, A.S., Singh, S., 2020. Photovoltaic–thermal (PV/T) technology: a comprehensive review on applications and its advancement. Int. J. Energy Environ. Eng. 11, 33–54. https://doi.org/10.1007/s40095-019-00327-y

Evans, D.L., 1981. Simplified method for predicting photovoltaic array output. Sol. energy 27, 555–560.

Good, C., 2016. Environmental impact assessments of hybrid photovoltaic–thermal (PV/T) systems–A review. Renew. Sustain. Energy Rev. 55, 234–239.

Haykin, S., 2007. Neural networks: a comprehensive foundation. Prentice-Hall, Inc.

Hazami, M., Riahi, A., Mehdaoui, F., Nouicer, O., Farhat, A., 2016. Energetic and exergetic performances analysis of a PV/T (photovoltaic thermal) solar system tested and simulated under to Tunisian (North Africa) climatic conditions. Energy 107, 78–94.

Ibrahim, A., Othman, M.Y., Ruslan, M.H., Mat, S., Sopian, K., 2011. Recent advances in flat plate photovoltaic/thermal (PV/T) solar collectors. Renew. Sustain. energy Rev. 15, 352–365. https://doi.org/10.1016/j.rser.2010.09.024

IEA PVPS, 2019. Trends in photovoltaic applications 2019, Task 1 Strategic PV analysis and outreach.

Joshi, A.S., Tiwari, A., Tiwari, G.N., Dincer, I., Reddy, B. V, 2009. Performance evaluation of a hybrid photovoltaic thermal (PV/T)(glass-to-glass) system. Int. J. Therm. Sci. 48, 154–164.

Kang, N., 2017. Multi-Layer Neural Networks with Sigmoid Function–Deep Learning for

630 Rookies. Towar. Data Sci.
631 Kumar, A., Baredar, P., Qureshi, U., 2015. Historical and recent development of photovoltaic
632 thermal (PVT) technologies. Renew. Sustain. Energy Rev. 42, 1428–1436.
633 https://doi.org/10.1016/j.rser.2014.11.044
634 Maria, M., Yassine, C., 2020. Machine learning based approaches for modeling the output
635 power of photovoltaic array in real outdoor conditions. Electron. 9, 315.
636 https://doi.org/10.3390/electronics9020315
637 Mojumder, J.C., Ong, H.C., Chong, W.T., Izadyar, N., Shamshirband, S., 2017. The
638 intelligent forecasting of the performances in PV/T collectors based on soft computing
639 method. Renew. Sustain. Energy Rev. 72, 1366–1378.
640 https://doi.org/10.1016/j.rser.2016.11.225
641 Patankar, S., 1980. Numerical heat transfer and fluid flow. Taylor & Francis.
642 Rejeb, O., Gaillard, L., Giroux-Julien, S., Ghenai, C., Jemni, A., Bettayeb, M., Menezo, C.,
643 2020. Novel solar PV/Thermal collector design for the enhancement of thermal and
644 electrical performances. Renew. Energy 146, 610–627.
645 https://doi.org/10.1016/j.renene.2019.06.158
646 Rojas, R., 1996. The backpropagation algorithm, in: Neural Networks. Springer, pp. 149–182.
647 Sarhaddi, F., Farahat, S., Ajam, H., Behzadmehr, A., 2010a. Exergetic performance
648 assessment of a solar photovoltaic thermal (PV/T) air collector. Energy Build. 42, 2184–
649 2199. https://doi.org/10.1016/j.enbuild.2010.07.011
650 Sarhaddi, F., Farahat, S., Ajam, H., Behzadmehr, A., Mahdavi Adeli, M., 2010b. An
651 improved thermal and electrical model for a solar photovoltaic thermal (PV/T) air
652 collector. Appl. Energy 87, 2328–2339. https://doi.org/10.1016/j.apenergy.2010.01.001
653 Schmidhuber, J., 2015. Deep learning in neural networks: An overview. Neural networks 61,
654 85–117.
655 Sellami, R., Amirat, M., Mahrane, A., Slimani, M.E.A., Arbane, A., Chekrouni, R., 2019.
656 Experimental and numerical study of a PV/Thermal collector equipped with a PV-
657 assisted air circulation system: Configuration suitable for building integration. Energy
658 Build. 190, 216–234. https://doi.org/10.1016/j.enbuild.2019.03.007
659 Su, D., Jia, Y., Huang, X., Alva, G., Tang, Y., Fang, G., 2016. Dynamic performance analysis
660 of photovoltaic-thermal solar collector with dual channels for different fluids. Energy
661 Convers. Manag. 120, 13–24. https://doi.org/10.1016/j.enconman.2016.04.095
662 Swinbank, W.C., 1963. Long-wave radiation from clear skies. Q. J. R. Meteorol. Soc. 89,
663 339–348.

Tonui, J.K., Tripanagnostopoulos, Y., 2008. Performance improvement of PV/T solar collectors with natural air flow operation. Sol. Energy 82, 1–12. https://doi.org/10.1016/j.solener.2007.06.004

Tonui, J.K., Tripanagnostopoulos, Y., 2007. Improved PV/T solar collectors with heat extraction by forced or natural air circulation. Renew. Energy 32, 623–637. https://doi.org/10.1016/j.renene.2006.03.006

Touafek, K., Haddadi, M., Malek, A., 2013. Design and modeling of a photovoltaic thermal collector for domestic air heating and electricity production. Energy Build. 59, 21–28. https://doi.org/10.1016/j.enbuild.2012.10.037

Varol, Y., Koca, A., Oztop, H.F., Avci, E., 2010. Forecasting of thermal energy storage performance of Phase Change Material in a solar collector using soft computing techniques. Expert Syst. Appl. 37, 2724–2732. https://doi.org/10.1016/j.eswa.2009.08.007

Villalva, M.G., Gazoli, J.R., Filho, E.R., 2009. Comprehensive Approach to Modeling and Simulation of Photovoltaic Arrays. IEEE Trans. Power Electron. 24, 1198–1208. https://doi.org/10.1109/TPEL.2009.2013862

Waliullah, M., Hossain, M.Z., Saha, S., 2015. On the implementation of two-diode model for photovoltaic-thermal systems. Procedia Eng. 105, 725–732. https://doi.org/10.1016/j.proeng.2015.05.063

Yang, T., Athienitis, A.K., 2014. A study of design options for a building integrated photovoltaic/thermal (BIPV/T) system with glazed air collector and multiple inlets. Sol. Energy 104, 82–92. https://doi.org/10.1016/j.solener.2014.01.049

Yilmaz, S., Majcen, D., Heidari, M., Mahmoodi, J., Brosch, T., Patel, M.K., 2019. Analysis of the impact of energy efficiency labelling and potential changes on electricity demand reduction of white goods using a stock model: The case of Switzerland. Appl. Energy 239, 117–132.

Yu, Y., Yang, H., Peng, J., Long, E., 2019. Performance comparisons of two flat-plate photovoltaic thermal collectors with different channel configurations. Energy 175, 300–308. https://doi.org/10.1016/j.energy.2019.03.054